Journal of Mineralogical and Petrological Sciences (2025) 120:021

Amaterasuite, $Sr_4Ti_6Si_4O_{23}(OH)Cl$, a new mineral from jadeitite, a representative stone of Japan

Daisuke NISHIO-HAMANE[*], Mariko NAGASHIMA[**], Yuki MORI[***], Masayuki OHNISHI[†], Norimasa SHIMOBAYASHI[‡], Takashi MATSUMOTO[§] and Mitsuo TANABE[#]

[*]*Institute for Solid State Physics, the University of Tokyo, Kashiwa 277-8581, Japan*
[**]*Division of Earth Science, Graduate School of Sciences and Technology for Innovation, Yamaguchi University, Yamaguchi 753-8512, Japan*
[***]*Diffraction and Scattering Division, Japan Synchrotron Radiation Research Institute, Sayo 679-5198, Japan*
[†]*Takehana Ougi-cho, Yamashina, Kyoto 607-8082, Japan*
[‡]*Department of Geology and Mineralogy, Graduate School of Science, Kyoto University, Kyoto 606-8502, Japan*
[§]*Application Laboratories, Rigaku Corporation, Tokyo 196-8666, Japan*
[#]*Niimi, Okayama 718-0011, Japan*

Amaterasuite is a new mineral found in jadeitite, a representative stone of Japan, and was thus named after Amaterasu Omikami, one of the most important goddesses in Japanese mythology, as a tribute to Japanese stone culture. The new mineral was found in the Osayama mountain area, Osa-osakabe, Niimi City, Okayama Prefecture, Japan. Amaterasuite appears as bundles consisting of needle- to plate-shaped crystals as large as 150 μm around rutile. The Mohs hardness is 6. Its tenacity is brittle, and its calculated density is 4.0 g·cm^{-3}. Under plane-polarized light, the mineral is pleochroic, changing from blue to brown. The empirical formula, calculated on the basis of 23 O + 2 (OH,Cl) atoms per formula unit, is $(Sr_{3.32}Ba_{0.64})_{\Sigma 3.96}(Ti_{5.73}Fe_{0.16}Nb_{0.02})_{\Sigma 5.91}Si_{4.15}O_{23}(OH)_{0.95}Cl_{1.05}$; thus, its ideal formula is $Sr_4Ti_6Si_4O_{23}(OH)Cl$. The unit-cell parameters refined by powder X-ray diffraction using 80 peaks with large *d*-values are $a = 5.85558(2)$ Å, $b = 20.43960(8)$ Å, $c = 33.28240(12)$ Å, and $V = 3983.43(3)$ Å^3 ($Z = 8$) in the orthorhombic *Fddd* space group. The structure of amaterasuite from the metajadeitite area was fully identified as amaterasuite-4*O*, which is characterized by its dual nature, encapsulating two types (A and B) within a unit cell. The occupancy rates of the A and B types were estimated to be ~ 85 and ~ 15%, respectively. The refined site occupancies at the SrA and BaB sites indicate a strong site preference for Sr, similar to the preferential site occupancies in synthetic titanosilicate compounds.

Keywords: Amaterasuite, Jadeitite, New mineral, Amaterasu Omikami, Japan

INTRODUCTION

Jadeitite is a nearly monomineralic rock composed mainly of jadeite. Because of its strength and toughness, it was used as a hammer stone ~ 7000 years ago during the Jomon period in Japan, and this use of jadeitite is one of the oldest jadeite cultures in the world (Niigata Prefecture Archeological Research Corporation, 2006). Recent evidence suggests that jadeitite is formed only at divergent plate boundaries with cold temperature gradients, such as the Japanese islands, where aqueous fluids rising from the subducting oceanic crust condense to form jadeitite (e.g., Harlow et al., 2015). In recognition of the scientific importance and the preciousness of jadeitite, the Japan Association of Mineralogical Sciences designated 'jadeite (jadeitite)' as the national stone of Japan in September 2016 (Tsuchiyama, 2017). A comprehensive petrological understanding of Japanese jadeitite is summarized in the

doi:10.2465/jmps.250420
D. Nishio-Hamane, hamane@issp.u-tokyo.ac.jp Corresponding author

works of Tsujimori (2017) and Tsujimori and Harlow (2017). Japanese jadeitite corresponds to the oldest known jadeitite, and the latest related study reported that the Osayama jadeitite formed 523.6 ± 3.5 Ma (Peverelli et al., 2025).

In Japan, jadeitite has been found in the Itoigawa, Wakasa, and Osayama areas and is characterized by the occurrence of Sr-rich accessory minerals. Itoigawaite [$SrAl_2Si_2O_7(OH)_2 \cdot H_2O$], rengeite [$Sr_4Ti_4ZrO_8(Si_2O_7)_2$], and matsubaraite [$Sr_4Ti_5O_8(Si_2O_7)_2$] were found as new minerals from the Itoigawa jadeitite (Miyajima et al., 1999, 2001, 2002). Sr-bearing titanosilicates ohmilite [$Sr_3(Ti,Fe^{3+})(Si_2O_6)_2(O,OH) \cdot 2H_2O$] and strontio-orthojoaquinite [$NaSr_4Fe^{3+}Ti_2Si_8O_{24}(OH)_4$] have also been discovered as new minerals in albitite associated with the Itoigawa jadeitite (Komatsu et al., 1973; Chihara et al., 1974; Wise, 1982). In the prehnite rock in the Itoigawa area, niigataite [$CaSrAl_3(Si_2O_7)(SiO_4)O(OH)$] was found as a new member of the epidote group (Miyajima et al., 2003). Among them, itoigawaite was also found in the Wakasa jadeitite (Shimobayashi and Yamada, 2003). Recently, Nishio-Hamane and Tanabe (2021) reported the occurrence of matsubaraite and rengeite in the Osayama jadeitite. Their report also indicated the occurrence of an undetermined Sr-rich mineral, which was subsequently approved as a new mineral, amaterasuite, with composition $Sr_4Ti_6Si_4O_{23}(OH)Cl$.

The relationship between jadeitite and the Japanese people dates to ancient times. Today, jadeitite is recognized as a representative stone of Japan, and amaterasuite is a new mineral discovered among these symbolic stones. Therefore, as a tribute to Japanese stone culture, the new mineral, amaterasuite, was named after Amaterasu Omikami (also known as Amaterasu for short), the goddess of the sun in Japanese mythology. Her name appears in 'Kojiki' and 'Nihon Shoki', the oldest chronicles in Japanese history, compiled around 710–720 AD. The commonality of duality was also one of the reasons for the naming: Amaterasu has a duality of spirits, Ara-Mitama (wild spirit) and Nigi-Mitama (gentle spirit), and amaterasuite has a dual nature in its crystal structure (described below). The mineral and its name of amaterasuite (IMA No. 2024-056) have been approved by the International Mineralogical Association, Commission on New Minerals, Nomenclature, and Classification. The holotype specimen has been deposited in the collection of the National Museum of Nature and Science, Japan (NSM M-52596).

OCCURRENCE

The type locality (35°05′38″N 133°33′01″E) is located at the northeastern part of the Osayama mountain area, Osakabe, Niimi City, Okayama Prefecture, Japan, where jadeitite and its related rocks are distributed in association with serpentinite mélange (e.g., Tsujimori, 1998). There, one of the authors, M.T., found a ~ 1 m jadeitite block buried at the boundary between serpentinite and rodingite (Supplementary Fig. S1; Figs. S1–S3 are available online from https://doi.org/10.2465/jmps.250420). Most of the block was composed of jadeite, while the area in contact with the rodingite contained a substantial amount of prehnite, which we refer to as the metajadeitite area. It is noted that 'metajadeitite' is not a common petrological term, but a classification term in this paper. Jadeitite also contained veins of edenite; however, in the metajadeitite area, edenite disappeared and was replaced by chlorite (Fig. S1). By contrast, rutile contained in jadeitite remained even in the metajadeitite. Amaterasuite occurs in both jadeitite and metajadeitite, although their occurrence and appearance differ.

In jadeitite, rutile is often surrounded by titanite, forming rutile (core) + titanite (rim) aggregates as large as ~ 1 mm (Fig. 1a). Amaterasuite occurs by filling fine cracks a few micrometers wide in rutile, and the Sr-Ba minerals such as matsubaraite, tausonite, and henrymeyerite occur in common formations similar to amaterasuite (Fig. 1b). These minerals can only be observed by electron microprobe and distinguished by analysis because of their small size and lack of color. In rutile, amaterasuite is distributed discontinuously along the cracks; individual grains cannot be recognized. The same features are observed in other Sr-Ba minerals.

In the metajadeitite area, rutile (core) + titanite (rim) aggregate remains. However, most of the cracks in rutile are replaced by titanite; thus, the occurrence of Sr-Ba minerals becomes scarce. Amaterasuite is also rarely found in the cracks in rutile; it is instead found in the titanite rim (Figs. 1c and 1d). In this occurrence, amaterasuite is larger than that in jadeitite, reaching more than 100 μm, and can be observed with an optical microscope. For the other Sr-Ba minerals, the difference in the occurrence of tausonite is remarkable. It occurs mainly at the boundary between rutile and titanite and on the outer edge of titanite; in addition, the grains have grown significantly. As a result, in the metajadeitite area, aggregates of rutile, titanite + amaterasuite, and tausonite are occasionally found because their appearance differs from that of simple rutile (Fig. S2).

These occurrences suggest that there may be multiple reaction pathways to the formation and growth of amaterasuite, whereas all occurrences appear to start with rutile, a common mineral often associated with jadeitite. Because the occurrences are very small and few, amaterasuite may be a common but often overlooked mineral in rutile-bearing jadeitite.

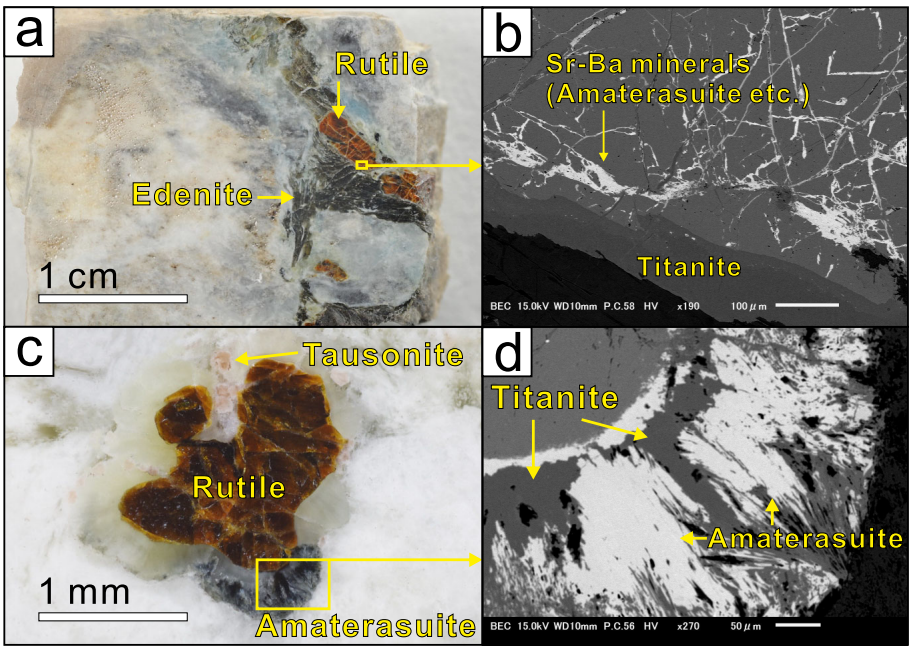

Figure 1. The representative occurrence of amaterasuite from jadeitite [(a) and (b)] and the metajadeitite area [(c) and (d)]. Amaterasuite often occurs by filling cracks in rutile in association with Sr-Ba minerals in jadeitite [(a) and (b)], whereas it occurs in titanite surrounding rutile in the metajadeitite area [(c) and (d)].

PHYSICAL AND OPTICAL PROPERTIES

Amaterasuite, which can be observed with an optical microscope, is only found in the metajadeitite area, and its properties are described here. Amaterasuite often appears as bundles consisting of needle- to plate-shaped crystals as large as 150 μm. The mineral has a transparent deep-blue to green color with vitreous luster, whereas its streak is white. Amaterasuite is nonfluorescent, brittle, and uneven in fracture. Cleavage or parting could not be determined. Its Mohs hardness, as measured by rubbing a reference mineral powder against a sample fixed onto a glass slide, is 6. Its density is 4.0 g·cm^{-3}, as calculated from the empirical formula and single-crystal X-ray diffraction (XRD) data.

The refractive indices (α, β, and γ) of amaterasuite are all in the range between 1.81 (methylene iodide + sulfur + tetraiodoethylene) and 2.30 (sulfur-selenium melt). Although a specific value could not be determined because we did not have a medium with an adjustable refractive index, the mean refractive index obtained from the Gladstone-Dale relationship (Mandarino, 1981) using the empirical formula is 2.03, consistent with the observation ($1.81 < n < 2.30$). Amaterasuite is pleochroic, changing from blue to brown under plane-polarized light (Fig. S3). The orientation of the crystals could not be determined from the observations.

RAMAN SPECTROSCOPY

Raman spectroscopic analysis of amaterasuite from the metajadeitite area was carried out using a Renishaw inVia

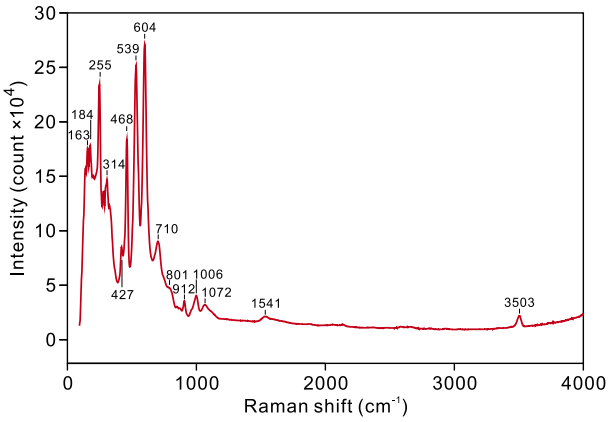

Figure 2. Raman spectrum of amaterasuite in the metajadeitite area.

Reflex spectrometer at the Institute for Solid State Physics, University of Tokyo (ISSP). The spectrum was obtained from 100 to 4000 cm^{-1} using a 532 nm diode laser (Fig. 2). The O-H stretching vibration at 3503 cm^{-1} is observed in the Raman spectra of amaterasuite, whereas the O-H bending mode (~ 1640 cm^{-1}) is not observed. Therefore, only the OH group is considered to be present in amaterasuite structure; no water molecules are present. Although several Raman bands are observed in the lattice-vibration region, their specific assignments remain unavailable.

CHEMICAL COMPOSITION

Chemical analyses for the type specimen were conducted using a JEOL JXA-8105 (WDS mode, 15 kV, 10 nA, 3

Table 1. Chemical compositions of amaterasuite

	In metajadeitite (type specimen) WDS analysis wt% (n = 22)			In jadeitite EDS analysis wt% (n = 5)	
	Avg.	Range		Avg.	Range
SiO_2	20.21	19.76–20.55	SiO_2	19.18	18.54–19.42
TiO_2	37.10	35.94–37.96	TiO_2	39.94	38.82–40.99
Fe_2O_3	1.01	0.65–1.53	Fe_2O_3	0.75	0.59–0.75
Nb_2O_5	0.19	0.04–0.37	Nb_2O_5	0.54	0.07–0.97
SrO	27.92	24.96–29.38	SrO	29.27	28.64–29.90
BaO	8.01	6.63–9.99	BaO	8.32	7.37–9.05
Cl	3.01	2.78–3.29	Cl	2.83	2.60–2.93
H_2O^*	0.70		H_2O^*	0.78	
–O = Cl	0.68		–O = Cl	0.64	
Total	97.47		Total	100.97	
	apfu			apfu	
Sr	3.32		Sr	3.39	
Ba	0.64		Ba	0.65	
Σ	3.96		Σ	4.04	
Ti	5.73		Ti	6.00	
Fe	0.16		Fe	0.11	
Nb	0.02		Nb	0.05	
Σ	5.91		Σ	6.16	
Si	4.15		Si	3.83	
O =	23		O =	23	
OH^{**}	0.95		OH^{**}	1.04	
Cl	1.05		Cl	0.96	
Σ =	2		Σ =	2	

* Calculated value from stoichiometry.
** OH is estimated as 2 − Cl.

μm beam diameter) at the Department of Geology and Mineralogy, Kyoto University. For other specimen, a JEOL IT-100 (EDS mode, 15 kV, 0.8 nA, 1 μm beam diameter) at ISSP was used. The ZAF method was used for data correction in both the WDS and EDS analyses. The standards used in these analyses were silicon for Si, tausonite for Sr and Ti, hematite for Fe, $LaNbO_4$ for Nb, $BaTiSi_3O_9$ for Ba, and $Ba_5(ReO_5)_3Cl$ for Cl. Although insufficient material was available for direct determination, single-crystal X-ray refinement indicated the presence of OH in the structure (also confirmed by Raman spectroscopy). Thus, the H_2O wt% was estimated by stoichiometry. The analytical data are shown in Table 1. The slightly low total wt% in WDS analysis is probably due to electron damage because the EDS measurements performed at low current did not result in a deficiency of wt%. However, the WDS values were adapted as new mineral data in the type specimen because it could avoid the Sr–Si and Ba–Ti peak overlaps. The empirical formula of type specimen amaterasuite from the metajadeitite area, as calculated on the basis of 23 O + 2 (OH,Cl), is $(Sr_{3.32}Ba_{0.64})_{\Sigma 3.96}(Ti_{5.73}Fe_{0.16}Nb_{0.02})_{\Sigma 5.91}Si_{4.15}O_{23}(OH)_{0.95}Cl_{1.05}$. The composition of amaterasuite in rutile in jadeitite is $(Sr_{3.39}Ba_{0.65})_{\Sigma 4.04}(Ti_{6.00}Fe_{0.11}Nb_{0.05})_{\Sigma 6.16}Si_{3.83}O_{23}(OH)_{1.04}Cl_{0.96}$. The ideal formula is $Sr_4Ti_6Si_4O_{23}(OH)Cl$, which requires SrO 35.41, TiO_2 40.95, SiO_2 20.53, H_2O 0.77, Cl 3.03, –O = Cl 0.68, and Total 100 wt%.

CRYSTAL STRUCTURE

Amaterasuite [$Sr_4Ti_6Si_4O_{23}(OH)Cl$] and a titanosilicate compound, $(Ba,Sr)_4Ti_6Si_4O_{24}\cdot H_2O$, reported by Cadoni et

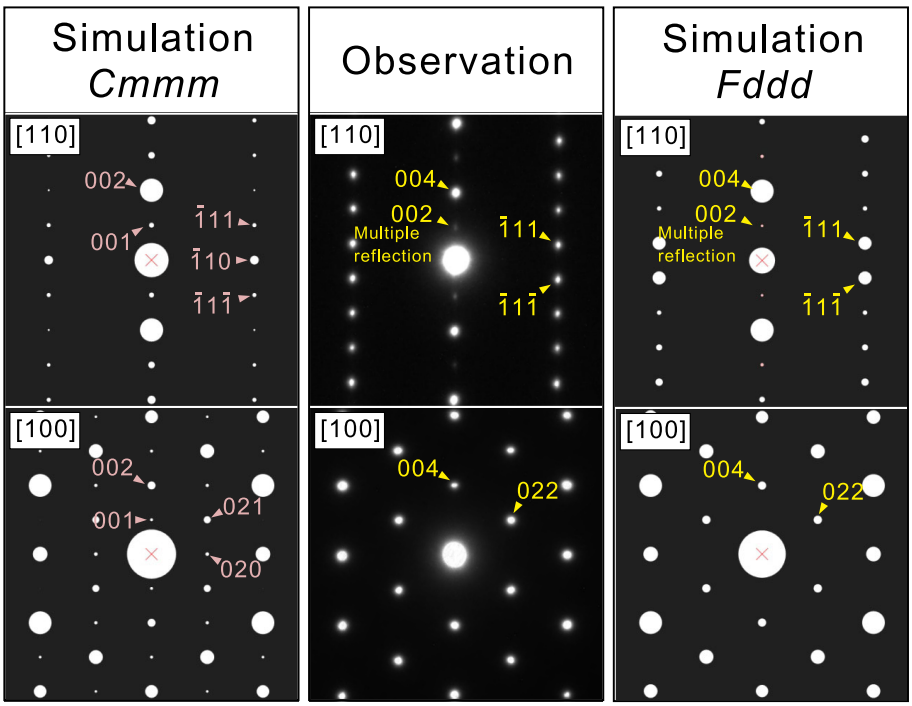

Figure 3. Observed and simulated selected-area electron diffraction patterns from [110] and [100] of amaterasuite from the metajadeitite area. The simulations were performed using the ReciPro program with dynamical theory (Seto and Ohtsuka, 2022). The observed electron diffraction patterns of amaterasuite are understood only under the *Fddd* model. In space group Fddd, the 002 reflection violates the extinction rules, but can occur due to multiple reflections (e.g., when the origin is moved to a reflection in the left or right column).

al. (2008) have similar stoichiometry in terms of 4Sr(Ba) + 6Ti + 4Si and 25(O + Cl); they are therefore structurally related. The structure of the titanosilicate compound was solved as a disordered structure of the orthorhombic *Cmmm* space group (a = 5.906 Å, b = 20.618 Å, and c = 16.719 Å) and was then deciphered to an ordered structure of the monoclinic $P2/c$ space group (a = 5.906 Å, b = 16.719 Å, c = 10.724 Å, and β = 105.99°) on the basis of the order-disorder theory developed by Dornberger-Schiff (1964) and Ferraris et al. (2004). However, another polytype with different stacking sequences has been proposed: the 4*O* polytype with a disordered structure of the orthorhombic *Fddd* space group with a ***c***-axis length approximately twice that of the *Cmmm* space-group model ($c \sim 33.5$ Å). Cadoni et al. (2008) mentioned this 4*O* polytype, although they did not refine the structure, because it was not present in their titanosilicate compounds.

Electron diffraction

Polytypes are occasionally intermixed. Thus, we investigated the crystal quality by electron diffraction using a transmission electron microscope (JEOL JEM-2100, operating at 200 kV) at ISSP. Samples were prepared using amaterasuite from the metajadeitite area by Ar^{+}-ion milling using an ion-slicer (JEOL EM-09100IS).

All of the electron diffraction patterns for amaterasuite could be indexed to the orthorhombic symmetry. Figure 3 shows the observed and simulated electron diffraction patterns from [110] and [100], which are key to determining the polytype. The observed electron diffraction patterns of amaterasuite are clearly consistent with the *Fddd* space-group model. In addition, because no spots or streaks indicative of other polytypes were observed, amaterasuite from the metajadeitite area can be regarded as a single phase of the 4*O* polytype.

X-ray diffraction

The XRD data for a single crystal of amaterasuite were collected with Mo*K*α radiation using an XtaLAB Synergy-R/DW equipped with VariMax DW optics and a HyPix6000HE detector (Rigaku), located at the Center for Instrumental Analysis, Yamaguchi University. The crystal sample from the metajadeitite area was mounted onto a glass fiber, and intensity data were collected at room temperature. Preliminary unit-cell parameters and an orientation matrix were obtained from six sets of frames and were refined during the integration process of the intensity data. The diffraction data and empirical absorption correction were processed using CrysAlis^{Pro} (Matsumoto et al., 2021). The SHELXL-2019/3 software (Sheldrick, 2015) was used for refinement of the crystal structure with neutral atom-scattering factors. The reflection statistics and systematic absences were set to the *Fddd* space group, as confirmed by the electron diffractions. The structure model was then solved using the direct method.

During the process of crystal structure refinement, the

Table 2. Experimental details of the single-crystal XRD analysis of amaterasuite

Crystal size (mm)		0.02 × 0.04 × 0.06
Space group		*Fddd*
Unit-cell dimensions	a (Å)	5.8603(2)
	b (Å)	20.4616(7)
	c (Å)	33.281(1)
	V (Å^3)	3990.75(2)
D_{calc} (g/cm^3)		4.02
Radiation		Mo$K\alpha$ (λ = 0.71073 Å)
Monochromator		VariMax optics
Diffractometer		Rigaku XtaLAB Synergy-R/DW with HyPix-6000HE
Scan type		ω scan
Absorption correction		CrysAlis^{Pro} (Matsumoto et al., 2021)
Absorption coefficient μ (mm^{-1})		12.83
θ_{min}-θ_{max}(°)		2.3-36.3
Collected reflections		12346
Unique reflctions		2393
R_{int} (%)		6.82
Index ranges	h	−9 → 9
	k	−33 → 34
	l	−55 → 55
Refinement on F^2 using		SHELXL-2019/3 (Sheldrick, 2015)
R_1 (%)		5.03
wR_2 (%)		11.75
No. of parameters		136
Weighting scheme*		$w = 1/[\sigma^2(F_o^2) + (0.0454P)^2 + 54.10P]$
$\Delta\rho_{max}$ (e Å^{-3})		1.09 at 0.90 Å from O2A
$\Delta\rho_{min}$ (e Å^{-3})		−1.32 at 0.89 Å from SrA

* The function of the weighting scheme is $w = 1/[\sigma^2(F_o^2) + (a \cdot P)^2 + b \cdot P]$, where $P = [\mathrm{Max}(F_o^2) + 2F_c^2]/3$, and the parameters a and b are chosen to minimize the differences in the variances for reflections in different ranges of intensity and diffraction angle.

hydrogen position (H6A) of the hydroxyl groups around O6 was derived from difference-Fourier synthesis. However, the O6-H6A configuration means that both the donor and the acceptor are O6. Thus, the occupancy of hydrogen at H6A was fixed as 0.25 from a stoichiometric perspective. The displacement parameter of the H atom was fixed as the value of U_{iso} = 0.05 Å^2, with a restraint of O-H = 0.980(1) Å applied (Franks, 1973). The displacement parameters of the other atoms were analyzed anisotropically, whereas that of the O2B site resulted in a large value, which was reported as alert level A by checkCIF. This issue can be avoided by analyzing U_{iso} or by fixing the value obtained at the O2A site. However, because the parameters converged to positive values, we used the results of anisotropic refinement. The refinement converged to R_1 = 5.03% for 2393 unique reflections with $I > 2\sigma_1$.

Details related to the sample, data collection, and structure refinement are provided in Table 2 and Supplementary CIF file (Supplementary CIF file is available online from https://doi.org/10.2465/jmps.250420). The final atom coordinates and equivalent isotropic atomic displacement parameters are summarized in Table 3. Selected interatomic distances are shown in Table 4, and bond valences are reported in Table 5. The refined unit-cell parameters were a = 5.8603(3), b = 20.4616(7), c = 33.2810(12) Å, and V = 3990.8(2) Å^3 (Z = 8) in the orthorhombic *Fddd* (#70-2) space group.

Synchrotron powder XRD patterns were collected using a large Debye-Scherrer camera equipped with MYTHEN2 detectors and installed at the powder diffraction BL02B2 beamline of SPring-8, Hyogo, Japan (Kawaguchi et al., 2017). Rock samples of the metajadeitite area were roughly crushed, and the target minerals were then selected. Powder samples were packed into a borosilicate glass capillary with an outer diameter of 0.3 mm and a glass wall thickness of 0.01 mm. The wavelength of the incident X-rays was determined to be λ = 0.93186 Å using a CeO_2 standard. Measurements were performed at room temperature (296 K) with an exposure time of 600 s.

The XRD pattern showed the presence of titanite and

Table 3. Refined atomic positions with occupancy and anisotropic displacement parameters (Å^2) of amaterasuite

	W	*x*	*y*	*z*	U^{eq}	Occupancy
SrA	32*h*	0.61652(7)	0.52278(2)	0.56069(2)	0.01249(12)	$Sr_{0.746(6)}Ba_{0.104}$
BaB	32*h*	0.1311(5)	0.52238(13)	0.56073(9)	0.0277(8)	$Ba_{0.078(5)}Sr_{0.072}$
Ti1A	32*h*	0.1309(4)	0.38506(6)	0.52604(5)	0.0140(3)	$Ti_{0.85}$
Ti1B	32*h*	0.115(3)	0.3648(4)	0.5255(4)	0.0220(19)	$Ti_{0.15}$
Ti2	16*g*	7/8	3/8	0.62409(3)	0.00906(19)	$Ti_{1.0}$
Si1A	16*f*	1/8	0.51347(8)	5/8	0.0076(3)	$Si_{0.85}$
Si2A	16*g*	1/8	5/8	0.55867(5)	0.0075(3)	$Si_{0.85}$
Si1B	16*f*	5/8	0.5137(6)	5/8	0.018(2)	$Si_{0.15}$
Si2B	16*g*	5/8	5/8	0.5582(4)	0.020(2)	$Si_{0.15}$
O1	32*h*	0.1284(5)	0.37254(14)	0.58594(9)	0.0125(5)	$O_{1.0}$
O2A	32*h*	0.1373(8)	0.55874(18)	0.58503(13)	0.0191(8)	$O_{0.85}$
O2B	32*h*	0.611(5)	0.5611(13)	0.5862(8)	0.031(6)	$O_{0.15}$
O3	32*h*	0.3644(5)	0.62733(16)	0.53397(9)	0.0148(5)	$O_{1.0}$
O4	32*h*	0.6216(6)	0.56155(15)	0.47632(9)	0.0128(5)	$O_{1.0}$
O5	32*h*	0.8860(5)	0.47248(13)	0.62393(10)	0.0127(5)	$O_{1.0}$
O6	32*h*	0.8726(6)	0.43962(16)	0.52656(10)	0.0149(6)	$O_{1.0}$
ClA	8*b*	5/8	5/8	5/8	0.0163(4)	$Cl_{0.85}$
ClB	8*a*	1/8	5/8	5/8	0.018(2)	$Cl_{0.15}$
H6A	32*h*	0.961(10)	0.469(2)	0.5095(16)	0.05 U_{iso}	$H_{0.25}$
	U^{11}	U^{22}	U^{33}	U^{12}	U^{13}	U^{23}
SrA	0.01148(19)	0.01007(18)	0.0159(2)	−0.00379(13)	−0.0005(2)	−0.00033(18)
BaB	0.0295(14)	0.0240(13)	0.0294(14)	−0.0037(9)	0.0032(15)	−0.0010(13)
Ti1A	0.0205(6)	0.0136(6)	0.0078(4)	−0.0006(5)	0.0000(5)	−0.0074(6)
Ti1B	0.033(4)	0.021(4)	0.012(3)	−0.005(4)	−0.004(3)	−0.014(5)
Ti2	0.0097(4)	0.0075(3)	0.0100(4)	0	0	−0.0008(3)
Si1A	0.0062(7)	0.0075(7)	0.0092(7)	0	0.0009(8)	0
Si2A	0.0054(7)	0.0096(7)	0.0074(7)	0	0	0.0001(7)
Si1B	0.014(5)	0.024(6)	0.017(5)	0	0.007(6)	0
Si2B	0.030(6)	0.007(4)	0.023(6)	0	0	0.004(5)
O1	0.0101(12)	0.0171(12)	0.0103(11)	0.0006(10)	−0.0002(11)	0.0002(17)
O2A	0.0217(19)	0.0126(15)	0.0231(19)	0.0081(14)	0.000(2)	−0.0018(17)
O2B	0.035(15)	0.029(13)	0.029(13)	0.002(10)	0.010(14)	−0.029(13)
O3	0.0107(13)	0.0243(15)	0.0094(11)	0.0003(11)	−0.0004(11)	0.0019(17)
O4	0.0086(12)	0.0138(12)	0.0159(13)	0.0008(10)	−0.0013(15)	−0.0008(13)
O5	0.0115(12)	0.0108(11)	0.0158(12)	−0.0011(10)	0.0007(15)	0.0002(9)
O6	0.0096(12)	0.0171(13)	0.0180(15)	0.0005(11)	−0.0002(15)	0.0023(13)
ClA	0.0201(11)	0.0135(9)	0.0151(10)	0	0	0
ClB	0.015(6)	0.018(6)	0.020(6)	0	0	0

tausonite in addition to amaterasuite because of its occurrence; thus, we applied the Le Bail analysis for peak identification using the JANA2006 software (Petříček et al., 2014). The pattern fitting under the three-phase model converged to R_{wp} = 2.44% (Fig. 4), and 370 peaks of amaterasuite were identified in the 5° ≤ 2θ ≤ 50° range. The lattice parameters refined by least-squares fitting using 80 peaks with a large *d*-value were *a* = 5.85558(2) Å, *b* = 20.43960(8) Å, *c* = 33.28240(12) Å, and *V* = 3983.43(3) Å^3 (Supplementary Table S1; Table S1 is available online from https://doi.org/10.2465/jmps.250420). The parameters [*d* in Å ($I_{obs.}$) *hkl*] for the seven observed strongest lines of amaterasuite in the 5° ≤ 2θ ≤ 50° range (11 ≥ *d* ≥ 1.1 Å) of the powder XRD pattern were 3.3374 (83) 062, 3.2454 (78) 137, 3.2262 (87) 048, 3.1647 (100) 0 2 10, 2.8835 (74) 202, 2.2204 (87) 260, and 1.3051 (76) 2 10 16.

Discussion

Figure 5 shows the whole crystal structure of amatera-

Table 4. Selected bond distances in amaterasuite

Type A			Type B		
SrA-	O1	3.090(3)	BaB-	O1	3.179(4)
	O2A	3.014(5)		O2B	3.04(3)
	O3	2.748(3)		O3	2.660(4)
	O3	2.731(3)		O3	2.697(4)
	O4	2.538(3)		O4	2.564(4)
	O4	2.918(3)		O5	2.763(4)
	O5	2.826(3)		O5	2.744(4)
	O5	2.826(3)		O6	2.540(4)
	O6	2.537(3)		O6	3.007(5)
	ClA	2.9930(6)		ClB	2.998(3)
	^{X}<SrA-O>	2.822		^{X}<BaB-O>	2.819
Ti1A-	O1	2.010(3)	T1B-	O1	2.019(12)
	O4	1.818(4)		O4	1.857(15)
	O3	2.006(3)		O3	1.996(12)
	O4	2.064(4)		O4	2.158(11)
	O6	1.881(4)		O6	1.783(12)
	O6	2.131(4)		O6	2.090(14)
	^{VI}<Ti1A-O>	1.985		^{VI}<Ti1B-O>	1.984
T2-	O1 (×2)	1.954(3)	T2-	O1 (×2)	1.954(3)
	O1 (×2)	1.965(3)		O1 (×2)	1.965(3)
	O5 (×2)	1.996(3)		O5 (×2)	1.996(3)
	^{VI}<Ti2-O>	1.972		^{VI}<Ti2-O>	1.972
Si1A-	O2A (×2)	1.623(4)	Si1B-	O2B (×2)	1.62(3)
	O5 (×2)	1.633(3)		O5 (×2)	1.748(7)
	^{IV}<Si1A-O>	1.628		^{IV}<Si1B-O>	1.68
Si2A-	O2A (×2)	1.617(4)	Si2B-	O2B (×2)	1.61(3)
	O3 (×2)	1.627(3)		O3 (×2)	1.728(7)
	^{IV}<Si2A-O>	1.622		^{IV}<Si2B-O>	1.67

suite. The framework of the structure is formed by octahedral ribbons and tetrahedral rings, and Sr(Ba) and Cl sites are located at cavities in the framework. The TiO_6 octahedra share a corner in the ***c***-axis direction, three of them make up one unit, and a continuous ribbon is formed in the ***a***-axis direction by sharing edges. One ring composed of four SiO_4 tetrahedra is located at the center of the four ribbons, and the ribbons and the ring share a corner. The Sr(Ba)-centered polyhedron is located between octahedral ribbons and tetrahedral rings. This polyhedron consists of nine oxygen atoms and one chlorine, connected by shared faces in the ***b***- and ***c***-axis directions and shared corners in the ***a***-axis direction, with four in one unit (Fig. 6).

However, the crystal structure exhibits a dual nature, encapsulating two types within a unit cell. Hence, the tetrahedral ring, Sr(Ba) sites, and Cl sites are characterized by the absence of one when the other is present. Figure 6 shows the details of the dual nature of the structure, where they are labeled as types A and B. The positional relationship between the types is a disorder at the Ti1 site and a 1/2 shift in the ***a***-axis direction for the other specific sites, marked as A or B. Because the sites for Ti and Si have less substitution relationship with other atoms, the occupancy rates of the A and B types were estimated using these sites. Conclusively, A and B were refined to be 85.1 ± 2.9 and 14.9 ± 2.9%; we fixed the occupancy of the A and B types at 85 and 15%, respectively. Then, the refined site occupancies at the SrA and BaB sites were found to be $Sr_{0.746(6)}Ba_{0.104}$ and $Ba_{0.078(5)}Sr_{0.072}$, respectively, indicating a strong Sr preference for the SrA site. Although the cause of this phenomenon is still unclear, a strong site

Table 5. Bond-valence analysis of amaterasuite weighted on the refined site occupancies*

	SrA	BaB	Ti1A	Ti1B	Ti2	Si1A	Si1B	Si2A	Si2B	Sum
O1	0.08	0.01	0.49	0.08	0.67×2↓ 0.65×2↓					1.98
O2A	0.10	0.02				0.85×2↓		0.87×2↓		2.14
O2B							0.15×2↓		0.16×2↓	
O3	0.17 0.18	0.04 0.04	0.49	0.09				0.84×2↓	0.11×2↓	1.96
O4	0.27 0.12	0.05	0.85 0.42	0.13 0.06						1.90
O5	0.14 0.14	0.03 0.03			0.60×2↓	0.83×2↓	0.11×2↓			1.88
O6	0.27	0.05 0.02	0.71 0.34	0.17 0.07						1.63
ClA	0.25×4→									1.20
ClB		0.05×4→								
Sum	2.07		3.90		3.84	3.88		3.96		

* The bond valence sums were calculated using the parameters of Brown and Altermatt (1985) and Gagné and Hawthorne (2015) for cation–Cl bonds and cation–O bonds, respectively.

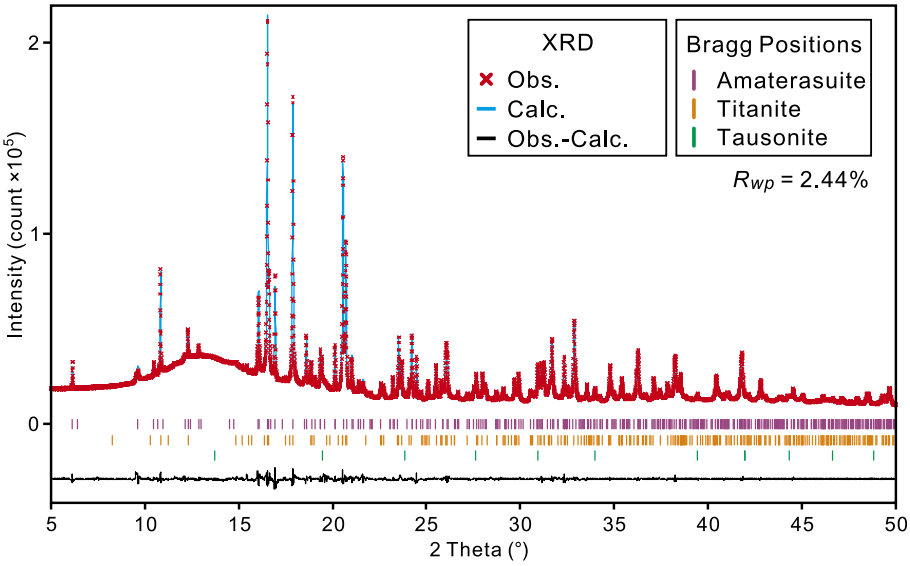

Figure 4. Result of full pattern fitting of the XRD pattern (λ = 0.93186 Å) of amaterasuite-bearing aggregate in the metajadeitite area using the Le Bail method.

preference for Sr has also been observed in the synthetic titanosilicate compound by Cadoni et al. (2008).

In this way, amaterasuite from the metajadeitite area was fully identified as the 4*O* polytype structure. Thus, the full notation of amaterasuite from metajadeitite is 'amaterasuite-4*O*' according to the polytype notation of Nickel (1993). The titanosilicate compounds in which other polytypes have been observed have compositions that slightly differ from that of amaterasuite, and the relationship between the former and the latter is Ba + O + H_2O and Sr + OH + Cl, respectively. The difference in the cation size and the charge balance at each site may have stabilized the 4*O* structure in amaterasuite from the metajadeitite area. Differences in origin may also affect the stability of the structure. To further verify these possibilities, it is important to systematically understand solid solutions, oc-

currence, and structure; however, the crystal structure of amaterasuite in rutile in jadeitite could not be determined because of its small size. This issue will be the subject of future study.

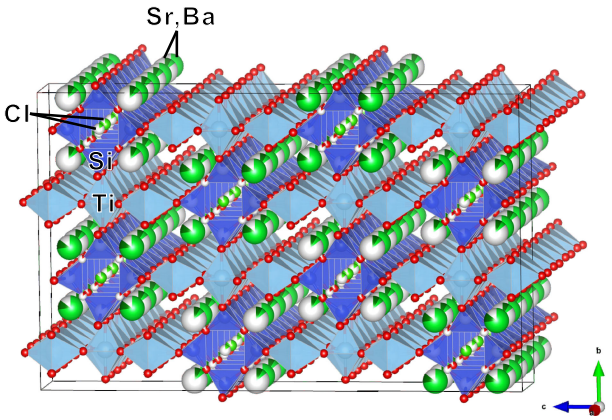

Figure 5. Whole crystal structure model of amaterasuite. The framework of the structure is formed by octahedral ribbons and tetrahedral rings, and Sr(Ba) and Cl sites are located at cavities in the framework. However, the crystal structure exhibits a dual nature, encapsulating two types within a unit cell. Hence, tetrahedral ring and Sr(Ba) and Cl sites are characterized by the absence of one when the other is present.

RELATIONSHIP TO OTHER MINERALS

Table 6 shows the Sr-bearing titanosilicate minerals found in jadeitite and its related rocks from Japan. Amaterasuite, matsubaraite, rengeite, ohmilite, and strontio-orthojoaquinite are listed. Among them, matsubaraite is most closely related to amaterasuite in terms of occurrence, composition, and structure. Compositionally, they share the same type of cation. They are also partially structurally related, particularly in the titanates, where both have triplet TiO_6 octahedra. In amaterasuite, the TiO_6 octahedra form unidirectionally bonded ribbons, whereas they form planarly bonded sheets in matsubaraite. Indeed, amaterasuite and matsubaraite have been observed to coexist in jadeitite. This sheet is also common to rengeite, with only isolated TiO_6 octahedra in matsubaraite being replaced by ZrO_6 octahedra in rengeite.

CONCLUSION

Amaterasuite is a new mineral with an ideal formula of $Sr_4Ti_6Si_4O_{23}(OH)Cl$. It is associated with jadeitite from Osayama. It was named after Amaterasu Omikami, the most important goddess in Japanese mythology, because it occurred from jadeitite, the symbol of Japanese stone

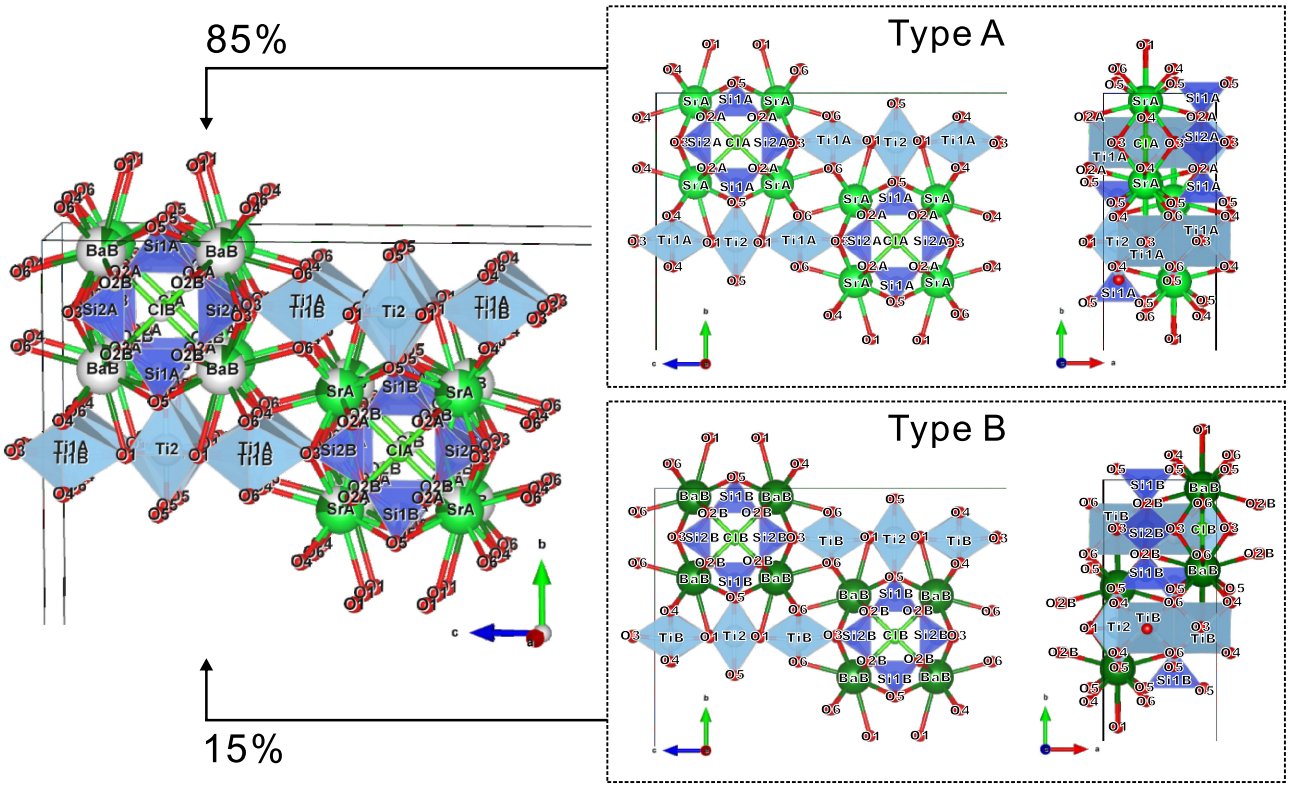

Figure 6. Pickup diagram of the crystal structure. The crystal structure of amaterasuite is constructed by synthesizing A- and B-type structures.

Table 6. Sr-bearing titanosilicate minerals found in jadeitite and its related rocks from Japan

Mineral name	Composition	Titanate feature			Ref.
		Unit	Connection	Host rock	
Amaterasuite	$Sr_4Ti_6Si_4O_{23}(OH)Cl$	Triplet	Ribbon	Jadeitite*	1
Matsubaraite	$Sr_4Ti_5O_8(Si_2O_7)_2$	Triplet, single	Sheet, Isolation	Jadeitite	2
Rengeite	$Sr_4Ti_4ZrO_8(Si_2O_7)_2$	Triplet	Sheet	Jadeitite	3
Ohmilite	$Sr_3(Ti,Fe^{3+})(Si_2O_6)_2(O,OH)\cdot 2H_2O$	Single	Chain	Albitite	4
Strontio-orthojoaquinite	$NaSr_4Fe^{3+}Ti_2Si_8O_{24}(OH)_4$	Pair	Dimer	Albitite	5

* including the metajadeitite area

1, This study; 2, Miyajima et al. (2002); 3, Miyajima et al. (2001); 4, Mizota et al. (1983); 5, Kato and Mizota (1990).

culture. Rutile is closely involved in the formation of amaterasuite. Amaterasuite from the metajadeitite area was fully identified as amaterasuite-4*O*, which is characterized by a dual nature within a single unit cell. The correspondence of their structure to amaterasuite in other occurrences remains a subject for future study. Among the Sr-bearing titanosilicate minerals occurring in jadeitite and related rocks, amaterasuite is closely related to matsubaraite in terms of occurrence, composition, and partial structure.

ACKNOWLEDGMENTS

Synchrotron radiation X-ray powder diffraction experiments were performed at SPring-8 with the approval of the Japan Synchrotron Radiation Research Institute (JASRI) (Proposal No. 2024A1895). This study used research equipment shared in the MEXT Project for Promoting Public Utilization of Advanced Research Infrastructure (Program for supporting construction of core facilities) Grant No. JPMXS0440400024 and was also supported by Core Clusters for Research Initiative of Yamaguchi University. One of the authors (M.N.) gratefully acknowledges the financial support of a Grant-in-Aid for Scientific Research from the Japan Society for the Promotion of Science, No. 23K03551.

SUPPLEMENTARY MATERIALS

Supplementary Figures S1-S3, Table S1, and CIF file are available online from https://doi.org/10.2465/jmps.250420.

REFERENCES

Brown, I.D. and Altermatt, D. (1985) Bond-valence parameters obtained from a systematic analysis of the inorganic crystal structure database. Acta Crystallographica, B41, 244-247.

Cadoni, M., Bloise, A., Ferraris, G. and Merlino, S. (2008) Order-disorder character and twinning in the structure of a new synthetic titanosilicate: $(Ba,Sr)_4Ti_6Si_4O_{24}\cdot H_2O$. Acta Crystallographica, B64, 669-675.

Chihara, K., Komatsu, M. and Mizota, M. (1974) A joaquinite-like mineral from Ohmi, Niigata Prefecture, Central Japan. Mineralogical Journal, 7, 395-399.

Dornberger-Schiff, K. (1964) Grundzüge einer Theorie von OD-Strukturen aus Schichten. Abhandlungen der Deutschen Akademie der Wissenschaften, Klasse für Chemie, Geologie und Biologie, 3, 107 (in German).

Ferraris, G., Makovicky, E. and Merlino, S. (2004) Crystallography of modular materials. Vol. 15, pp. 372, Oxford University Press, USA.

Franks, F. (1973) Water: A comprehensive treatise. Vol. 2, pp. 684, Plenum, New York.

Gagné, O.C. and Hawthorne, F.C. (2015) Comprehensive derivation of bond-valence parameters for ion pairs involving oxygen. Acta Crystallographica, B71, 562-578.

Harlow, G.E., Tsujimori, T. and Sorensen, S.S. (2015) Jadeitites and plate tectonics. Annual Reviews of Earth and Planetary Sciences, 43, 105-138.

Kato, T. and Mizota, T. (1990) The crystal structure of strontio-orthojoaquinite. Journal of the Faculty of Liberal Arts. Yamaguchi University, 24, 23-32.

Kawaguchi, S., Takemoto, M., Osaka, K., Nishibori, E., et al. (2017) High-throughput powder diffraction measurement system consisting of multiple MYTHEN detectors at beamline BL02B2 of SPring-8. Review of Scientific Instruments, 88, 085111.

Komatsu, M., Chihara, K. and Mizota, T. (1973) A new strontium-titanium hydrous silicate mineral from Ohmi, Niigata Prefecture, Central Japan. Mineralogical Journal, 7, 298-301.

Mandarino, J.A. (1981) The Gladstone-Dale relationship: Part IV. The compatibility concept and its application. The Canadian Mineralogist, 19, 441-450.

Matsumoto, T., Yamano, A., Sato, T., Ferrara, J.D., et al. (2021) "What is this?" a structure analysis tool for rapid and automated solution of small molecule structures. Journal of Chemical Crystallography, 51, 438-450.

Miyajima, H., Matsubara, S., Miyawaki, R. and Ito, K. (1999) Itoigawaite, a new mineral, the Sr analogue of lawsonite, in jadeitite from the Itoigawa-Ohmi district, central Japan. Mineralogical Magazine, 63, 909-916.

Miyajima, H., Matsubara, S., Miyawaki, R., Yokoyama, K. and Hirokawa, K. (2001) Rengeite, $Sr_4ZrTi_4Si_4O_{22}$, a new mineral, the Sr-Zr analogue of perrierite from the Itoigawa-Ohmi district, Niigata Prefecture, central Japan. Mineralogical Magazine, 65, 111-120.

Miyajima, H., Miyawaki, R. and Ito, K. (2002) Matsubaraite, $Sr_4Ti_5(Si_2O_7)_2O_8$, a new mineral, the Sr-Ti analogue of perrierite in jadeitite from the Itoigawa-Ohmi district, Niigata Prefecture, Japan. European Journal of Mineralogy, 14, 1119-1128.

Miyajima, H., Matsubara, S., Miyawaki, R. and Hirokawa, K. (2003) Niigataite, $CaSrAl_3(Si_2O_7)(SiO_4)O(OH)$: Sr-analogue of clinozoisite, a new member of the epidote group from the Itoigawa-Ohmi district, Niigata Prefecture, central Japan. Journal of Mineralogical and Petrological Sciences, 98, 118-129.

Mizota, T., Komatsu, M. and Chihara, K. (1983) A refinement of the crystal structure of ohmilite, $Sr_3(Ti,Fe^{3+})(O,OH)(Si_2O_6)_2 \cdot 2\text{-}3H_2O$. American Mineralogist, 68, 811-817.

Nickel, E.H. (1993) Standardization of polytype suffixes. The Canadian Mineralogist, 31, 767-768.

Niigata Prefecture Archeological Research Corporation (2006) The Ogakuchi site. pp. 85, Niigata Prefecture Archeological Research Report, 173 (in Japanese).

Nishio-Hamane, D. and Tanabe, T. (2021) Matsubaraite, rengeite, törnebohmite-(Ce) and rare minerals in Osayama jadeitite. 2021 Annual Meeting of Japan Association of Mineralogical Sciences, R1P-09 (in Japanese).

Petříček, V., Dušek, M. and Palatinus, L. (2014) Crystallographic Computing System JANA2006: General features. Zeitschrift für Kristallographie - Crystalline Materials, 229, 345-352.

Peverelli, V., Olivieri, O.S., Tsujimori, T., Giovannelli, D., et al. (2025) Cold-subduction biogeodynamics boosts deep energy delivery to the forearc. Geochimica et Cosmochimica Acta, 388, 195-207.

Seto, Y. and Ohtsuka, M. (2022) ReciPro: free and open-source multipurpose crystallographic software integrating a crystal model database and viewer, diffraction and microscopy simulators, and diffraction data analysis tools. Journal of Applied Crystallography, 55, 397-410.

Sheldrick, G.M. (2015) Crystal structure refinement with SHELX. Acta Crystallographica, C71, 3-8.

Shimobayashi, N. and Yamada, S. (2003) Coexistence of itoigawaite and pumpellyite in jadeitite from Wakasa district, Tottori Prefecture, Japan. Abstracts for Annual Meeting of the Mineralogical Society of Japan, k08-09 (in Japanese).

Tsuchiyama, A. (2017) Jadeite: The national stone of japan. Elements, 13, 51.

Tsujimori, T. (1998) Geology of the Osayama serpentinite melange in the central Chugoku Mountains, southwestern Japan:320 Ma blueschist-bearing serpentinite melange beneath the Oeyama ophiolite. The Journal of the Geological Society of Japan, 104, 213-231 (in Japanese with English abstract).

Tsujimori, T. (2017) Early Paleozoic jadeitites in Japan: An overview. Journal of Mineralogical and Petrological Sciences, 112, 217-226.

Tsujimori, T. and Harlow, G.E. (2017) Jadeitite (jadeite jade) from Japan: History, characteristics, and perspectives. Journal of Mineralogical and Petrological Sciences, 112, 184-196.

Wise, W.S. (1982) Strontiojoaquinite and bario-orthojoaquinite: two new members of the joaquinite group. American Mineralogist, 67, 809-816.

Manuscript received April 20, 2025
Manuscript accepted July 12, 2025
Advance online publication July 18, 2025
Released online publication August 7, 2025
Manuscript handled by Takahiro Kuribayashi